Electro-reduction of 2,4,6-Trinitrotoluene in Room Temperature Ionic Liquids: Evidence of an EC_2 Mechanism

Colin Kang,[a,b] *Junqiao Lee*[a], *Debbie S. Silvester*[a]*

[a] Nanochemistry Research Institute, Department of Chemistry, Curtin University, GPO Box U1987, Perth, 6845, Australia.

[b] Present address: School of Chemistry, Monash University, Clayton, Victoria 3800, Australia

*Email:d.silvester-dean@curtin.edu.au, Phone: +61(8)92667148

Submitted to: the Journal of Physical Chemistry C.

Abstract

The reduction of 2,4,6-trinitrotoluene (TNT) has been studied in eight room temperature ionic liquids (RTILs) on a gold (Au) microdisk electrode and a Au thin film-electrode (TFE). Three reduction peaks were observed in all RTILs, corresponding to the reductions of each of the three nitro groups in the TNT structure. TNT was the easiest to reduce in imidazolium RTILs, followed by pyrrolidiunum, then tetraalkylphosphonium. Diffusion coefficients (*D*) and electron counts (*n*) were calculated from potential-step chronoamperometry on the first reduction peak. *D*'s ranged from 0.7-4.1×10^{-11} m^2s^{-1}, and a plot of *D* against the inverse of viscosity was linear, indicating that the Stokes-Einstein relation holds well for TNT in RTILs. The electron count was 1 in most RTILs, in stark contrast to the widely accepted 6-electron reduction in protic solvents. An electrogenerated red solid was formed after the first reduction peak, believed to be an azo (or azoxy) compound formed by dimerization of two TNT radicals, although characterization of the product(s) proved difficult). The behaviour at different concentrations revealed different degrees of chemical reversibility of reduction peak. This evidence points towards the possibility of an EC_2 mechanism, which was supported by digital simulation of the experimental voltammograms. Understanding the reduction mechanism of TNT is essential if RTILs are to be used for TNT sensing applications, particularly at high concentrations.

1. Introduction

2,4,6-Trinitrotoluene (TNT) is an explosive compound commonly used for military, industrial, and mining applications. It has also been used in homemade explosives by terrorists due to its insensitivity to shock and friction (e.g. compared to other high explosives such as nitroglycerin), reducing the risk of accidental detonation. Additionally, if not completely removed after an explosion, its reduction products are known to be toxic and carcinogenic to humans and may contaminate drinking water.[1-3] Due to a range of security and environmental needs, the development of sensors for explosives such as TNT is of huge interest. Various techniques (both physical and chemical) have been developed to detect TNT, with electrochemical methods offering the advantages of low-cost instrumentation, portability, durability, sensitivity and rapid response times.[2,3] TNT is typically dissolved directly in the electrochemical solvent for sensing, or can be volatilized to be detected in the gas phase.[2,3]

From an electrochemical perspective, the presence of nitro groups on the aromatic ring results in TNT being redox active and able to accept electrons. The electrochemical reduction of TNT has therefore been studied extensively in aqueous media,[1,4-8] with the most accepted mechanism involving the transfer of 6 electrons and 6 protons in each reduction process (total of 18 electrons and 18 protons over the three processes).[1] Review articles on the electrochemical detection of TNT are also available.[2,3]

Despite the fact that the electrochemical behaviour of TNT has been well characterised in aqueous solvents, there has been very little work performed in aprotic solvents (e.g. acetonitrile), and also in room temperature ionic liquids (RTILs). Prabu et al.[9] reported the detection of TNT in acetonitrile using square wave stripping voltammetry (SWSV). Although their study was mostly analytical (i.e. no mechanistic investigations were performed), they mentioned that two peaks were observed on the reductive scan using cyclic voltammetry. In RTILs, Forzani et al.[10] reported cyclic voltammetry for the reduction of TNT in the RTIL 1-butyl-3-methylimidazolium

hexafluorophosphate ([C_4mim][PF_6]). Three reduction peaks were observed and the reduction processes were found to produce distinctive red coloured products, suggested to be azo and azoxy derivatives.[10] It was stated that the ionic liquid medium was essential to produce the coloured reaction products (since the same products were not observed in aqueous solutions) but a study on the reduction mechanism was not performed. A later study from the same group[11] also reported cyclic voltammetry for TNT reduction in [C_4mim][PF_6], again with no discussion on the mechanism. Fernandez et al.[12] reported differential pulse voltammetry (DPV) for TNT reduction on a screen-printed graphite electrode in the RTIL 1-hexyl-3-methylimidazolium bis(trifluoromethyl-sulfonyl)imide ([C_6mim][FAP]). Three reduction peaks were observed that scaled linearly with concentration, but again the reaction mechanism was not studied. Finally, Xiao et al.[13] observed three distinct reduction peaks for TNT in four RTILs using cyclic voltammetry (CV) and square wave voltammetry (SWV). They focussed on obtaining analytical parameters, reporting linear calibration curves (current vs. concentration) and limits of detection (LODs) for TNT (in solution and as vapors) in RTILs. They stated that the general nature of the reductive process was the same in RTILs as water, with a 6-electron, 6 proton reduction occurring at each peak. They suggested that the protons came from either water dissolved in the RTIL, or the acidic proton present on the imidazolium cation of the RTIL. However, evidence (e.g. electron counts, expected currents, simulation of peaks) was not provided to support their claim.

In this work, the reduction of TNT is studied in detail in a range of RTILs on gold microdisk and thin-film electrodes (TFEs). Calculation of diffusion coefficients and electron counts will reveal information on the diffusional properties of TNT in RTILs (c.f. Stokes-Einstein behaviour) and on the electrochemical reduction mechanisms, respectively. This work will also show the benefits of using miniaturised planar electrode devices, such as TFEs, for the detection of TNT with only very small (e.g. microliter) volumes of solvent.

2. Experimental

2.1 Chemical Reagents

The RTILs 1-ethyl-3-methylimidazolium bis(trifluoromethylsulfonyl)imide ([C_2mim][NTf_2]), 1-butyl-3-methylimidazolium bis(trifluoromethylsulfonyl)imide ([C_4mim][NTf_2]), *N*-butyl-*N*-methylpyrrolidinium bis(trifluoromethylsulfonyl)imide ([C_4mpyrr][NTf_2]) and trihexyltetradecylphosphonium bis(trifluoromethylsulfonyl)imide ([$P_{14,6,6,6}$][NTf_2]) were synthesized according to standard literature procedures[14,15] and kindly donated by the group of Professor Christopher Hardacre at Queens University, Belfast. The RTILs 1-hexyl-3-methylimidazolium trifluorotris(pentafluoroethyl)phosphate ([C_6mim][FAP]), 1-butyl-3-methylimidazolium hexafluorophosphate ([C_4mim][PF_6]), 1-butyl-3-methylimidazolium tetrafluroborate ([C_4mim][BF_4]) and trihexyltetradecylphosphonium pentafluoroethyltri-fluorophosphate ([$P_{14,6,6,6}$][NTf_2]) were purchased from Merck KGaA (Kilsyth, Victoria, Australia) at ultra-high purity electrochemical grade. All RTILs were used as received. Ultra pure water with a resistance of 18.2 MΩ cm (prepared by an ultra pure laboratory water purification system, Millipore Pty Ltd., North Ryde, NSW, Australia), acetonitrile (MeCN, Sigma–Aldrich, 99.8%), and acetone (Sigma-Aldrich, 99.9 %) solvents were used for washing the electrodes before and after use with RTILs. 2,4,6-Trinitrotoluene (TNT, 1000 µg/1 mL in acetonitrile) was purchased from Cerilliant Corporation, Round Rock, Texas, USA. Nitrogen gas was obtained from a gas line connected into the building (Curtin University) from a 99.99 % purity nitrogen gas cylinder and was used for purging. Ferrocene ($Fe(C_5H_5)_2$, 98 % purity) and tetra-*N*-butylammonium perchlorate (TBAP, 98 % purity) were purchased from Sigma Aldrich.

2.2 Instrumental

All electrochemical experiments were performed using either a µ-Autolab Type III potentiostat or PGSTAT101 Autolab potentiostat (both from Eco Chemie, Netherlands) interfaced to a PC with NOVA software. Experiments were carried out at a temperature of 294(±1) K. All experiments were carried out inside a custom-made aluminium Faraday cage contained inside a fume cupboard.

2.3 Microelectrode Experiments

A conventional two-electrode arrangement was employed, with a home-made gold microelectrode (12.7 µm radius) as the working electrode and a 0.5 mm diameter silver wire (Sigma Aldrich) as the combined counter and quasi-reference electrode. The microelectrode was polished on soft lapping pads (Buehler, Illinois) with alumina powder of decreasing size (3, 1 and 0.5 µm, Kemet, NSW, Australia) before electrochemical experiments. The electrode diameter was calibrated electrochemically by using steady-state voltammetry of a solution of 2 mM ferrocene (diffusion coefficient 2.3×10^{-9} m^2s^{-1} at 298K)[16] in acetonitrile with 0.1M TBAP. The electrodes were housed in a glass "T-cell" [17] designed for studying microlitre quantities (20 µL) of ionic liquids in a controlled environment. After the introduction of TNT to the RTIL, the cell was purged under high vacuum (Edwards high vacuum pump, Model ES 50) to remove any impurities in the ionic liquid (e.g. oxygen and dissolved water from atmospheric moisture).

2.4 Thin-film Electrode Experiments

Gold (Au) thin-film electrodes (TFEs), purchased from Micrux Technologies (Oviedo, Spain), consisted of a 1 mm diameter Au working electrode, platinum (Pt) quasi-reference electrode, and Pt counter electrode. The TFEs were electrochemically activated in a solution of 0.5 M H_2SO_4 by employing repetitive CV scans (ca. 50 cycles at 500 mVs^{-1}) over a potential range of -0.04 to 1.41 V, using an external Ag/AgCl reference electrode and Pt wire counter electrode. For making up solutions, appropriate volumes of TNT (in acetonitrile – from 1000 µg/1 mL stock solution) were added directly to the RTIL in a glass vial, and the acetonitrile was left to evaporate overnight in a vacuum chamber. Solutions involving ferrocene were similarly prepared (3 mM Fc in acetonitrile – stock solution) by adding Fc into the respective TNT/RTIL solutions before leaving under vacuum. 1.5 µL of this solution (either TNT or TNT plus Fc in the RTIL) was directly drop casted to cover the three electrodes. The TFEs were housed inside a glass cell (originally designed for gas experiments)[18] and purged under nitrogen gas for ~60 minutes to remove impurities in the ionic liquid (e.g. oxygen, dissolved water from atmospheric moisture, and any trace residual acetonitrile).

2.5 Chronoamperometric Experiments

Chronoamperometric transients were achieved using a sample time of 0.01s. The potential was stepped up from a position of zero current to a potential after the reduction peak was observed, and the current was measured for 10 s. A fit using the Shoup and Szabo expression[19] was performed using the software package Origin 6.0 (Microcal Software Inc.).

$$I = -4nFDcr_d f(t) \quad (1)$$

$$f(t) = 0.7854 + 0.8863t^{-1/2} + 0.2146e^{-0.7823t^{-1/2}} \quad (2)$$

$$t = \frac{4Dt}{r_d^2} \quad (3)$$

where n is the number of electrons transferred, F is Faraday's constant, D is the diffusion coefficient, c is the initial concentration of TNT, r_d is the radius of the microdisk electrode, τ is dimensionless time and t is the time. After deletion of the first few data points, 10 iterations were performed on the data, fixing the value for the electrode radius, which was previously calibrated. Once the fitting was optimised, the value for the diffusion coefficient (D) and the product of the number of electrons multiplied by the concentration (nc) was obtained.

Safety Considerations

TNT is a high explosive and is reactive at high temperature or pressure. It will detonate under strong shock, and also reacts with reducing agents. *Handling:* TNT is considered a hazardous chemical and should only be handled by trained individuals, under a chemical fume hood at all times. A lab coat, enclosed shoes, safety goggles and Viton gloves should be worn. *Storage:* TNT should be kept well away from initiators, protected from physical damage, separated from oxidizing materials, combustibles and sources of heat. *Disposal:* Hazardous waste generated from TNT should be stored in a separate container and transferred for disposal within 90 days.

3. Results and Discussion

In order to study the electrochemical reaction mechanism of TNT in RTILs, two Au electrodes of different sizes (conventional microdisk electrode, and macrodisk TFE) and eight different RTILs were employed. A detailed study is then carried out in one chosen ionic liquid on the TFE, by employing different concentrations of TNT, followed by digital simulation of the resulting voltametric responses.

3.1. Cyclic voltammetry of TNT reduction in RTILs on a microelectrode.

Figure 1 shows the reduction of ca. 3 mM TNT in 8 RTILs on a Au microdisk electrode (radius 12.7 μm) at a scan rate of 100 mVs^{-1}. A gold electrode was used in all experiments in this work (in contrast to platinum) since experiments displayed obvious fouling/passivation on Pt electrodes during TNT reduction scans; this fouling behaviour has also been documented before.[20] Three reduction peaks were observed in all RTILs (labelled as peaks I, II and III), likely to correspond to the reduction of the three nitro groups present on TNT, in accordance to previously reported data by other research groups in RTILs.[12,13] Very obvious peak-shaped responses (as opposed to steady-state behaviour) was observed, even at scan rates as slow as 10 mVs^{-1} (see Figure S1 in supporting information). This suggests that the diffusion coefficients of the species undergoing reduction are very slow (e.g. compared to e.g. ferrocene in RTILs, where steady-state behaviour was observed below 20 mVs^{-1} in $[C_4mim][NTf_2]$),[21] and this will be discussed in the next section when the diffusion coefficients are calculated.

The relative heights of the three reduction peaks was found to vary slightly over the eight RTILs, probably due to differences in solvation of the electrogenerated products, or different kinetics of the electrochemical step (and any follow-up chemical reactions). Generally, peak III appears to be more broad and drawn out compared to peaks I and II. At increased scan rates (Figure S1), peak I is easily distinguishable in all RTILs, but peaks II and III are more broad and begin to merge in some RTILs (e.g. in $[C_6mim][FAP]$ and $[P_{14,6,6,6}][NTf_2]$). It was found that the potential of peak I does not

change with respect to sweep rate (0.01 - 4 Vs^{-1}), whereas the potentials for peak II and III shifted to more negative values. This suggests that peak I is likely electrochemically reversible, and peaks II and III display some degree of quasi-reversibility. A plot of peak current (peak I) against the square root of scan rate was linear in all 8 RTILs, suggesting that the electrochemical reduction process is diffusion controlled. It was not possible to perform a similar analysis for peaks II and III due to the overlapping of current from peak I and merging at higher scan rates.

Due to the use of an unstable Ag wire reference electrode, the ferrocene/ferocenium (Fc/Fc^+) redox couple was used as an internal reference by adding ferrocene in-situ (CVs shown in Figure S2 of the supporting information). The potentials of peaks I, II and III vs. the midpoint of Fc/Fc^+ in all eight RTILs at 100 mVs^{-1} are given in Table 1. The potential of peak I is the lowest for all RTILs containing the imidazolium cation (-1.01 to -1.06 V), compared to the pyrrolidinium cation (-1.09 V) and the tetraalkylphosphonium cation (-1.13 to -1.14 V). This suggests that the RTIL cation stabilises the product of TNT reduction in the order: imidazolium, pyrrolidinium, phosphonium. A similar effect was reported for a rhenium-tetrazole complex in RTILs, where the reduction potentials were the most negative in RTILs with the $[P_{14,6,6,6}]^+$ cation. This variation in behaviour could be exploited in sensing applications for discriminatory analyte detection.

The peak-to-peak separations (ΔE_p) of peaks I, II and III relative to their oxidative back-peaks (where present) are shown in the supporting information along with the ΔE_p values for Fc/Fc^+. There is much more of a variation in ΔE_p for TNT compared to Fc/Fc^+ as the RTIL is changed, suggesting that the kinetics of the TNT reduction peaks are more affected by the nature of the RTIL compared to Fc/Fc^+. The larger than ideal (e.g. 60 mV) ΔE_p for Fc/Fc^+ is likely due to a combination of slower electron transfer kinetics in RTILs (rate constant of the order 10^{-3} cm s^{-1}) and the intermediate diffusion regimes (between steady-state convergent and transient linear diffusion) on microelectrodes in RTILs.[22] More close to ideal ΔE_p for Fc/Fc^+ in RTILs (ca. 70-75 mV) is observed on the larger electrode, which will be discussed in section 3.3. Although there is a

variation in ΔE_p values for TNT in the RTILs, it can generally be concluded that peak I exhibits relatively fast kinetics, peak II slightly slower kinetics and peak III much slower kinetics, consistent with observations of potential shifting at different scan rates (mentioned above).

3.2 Stokes-Einstein Behaviour of TNT in RTILs.

Further information on the properties of TNT in RTILs can be obtained by performing potential-step chronoamperometry on the first reduction peak. According to the Stokes-Einstein equation, the diffusion coefficient of a species is inversely proportional to the solvent viscosity: [23]

$$D = \frac{k_B T}{6\pi\eta a} \qquad (4)$$

Here, D = diffusion coefficient of the diffusing species, k_B = Boltzmann constant, T = temperature, η = solvent viscosity and a = hydrodynamic radius of the diffusing species. In RTILs, this general relationship (where D is proportional to the inverse of viscosity) holds well where the size of the diffusing species is close to (or larger than) the solvent molecules (e.g. ferrocene and cobaltocenium,[21] which have similar size to RTIL ions, and a large rhenium metal complex which was larger than the RTIL ions). However, the number on the denominator may be closer to 4 (the "sliding sphere" model) than 6, in some cases, and this is a topic of interest.[24-26] It is noted that this general relationship ($D \propto \eta^{-1}$) was found not to apply for small gas molecules[27-29] such as oxygen, sulfur dioxide and hydrogen, which may move through "voids" in the ionic liquid, with diffusion coefficients only partially dependent on the solvent viscosity. We will therefore investigate the Stokes-Einstein behavior for TNT in RTILs by calculating the diffusion coefficients in all eight RTILs using potential-step chronoamperometry on a microdisk electrode.

Chronoamperometric transients for the reduction of TNT at peak I for all eight RTILs are shown in Figure S3 of the supporting information. The potential was stepped from a position of

zero current (typically at 0 V) to a potential after peak I (but before the onset of peak II) and the current was measured for 10 seconds. The experimental transients were theoretically fitted to the Shoup and Szabo expression.[19] Excellent fitting was observed (shown in Figure S3) and the calculated diffusion coefficients are presented in table 2, in order of increasing viscosity of the RTIL. The diffusion coefficient of TNT (D_{TNT}) in RTILs can be compared to inorganic metal complexes such as ferrocene and a large rhenium-tetrazolato complex (e.g. D_{TNT} = 4.1 x 10^{-11} m^2 s^{-1} in [C_2mim][NTf_2], compared to D_{Fc} = 5.3 x 10^{-11} m^2 s^{-1} [21] and $D_{Re\text{-}tetrazole}$ = 8.1 x 10^{-12} m^2 s^{-1} [30] in the same RTIL), suggesting the size of TNT is somewhere in between the two. Figure 2 shows a plot of the diffusion coefficients of TNT in the eight RTILs vs. the inverse of viscosity of the RTIL. The linearity of the plot suggests that the diffusional behaviour of TNT in RTILs relates closely with the Stokes-Einstein equation (4). Assuming a value on the denominator of 6 (the "stick" limit) the hydrodynamic radius (α) of TNT in RTILs was calculated to be 0.179 nm (from the gradient of the plot in Figure 2). This compares well to the crystal structure calculation using Density Functional Theory (DFT), which gave a value of α = 0.185 nm for TNT. This was calculated by measuring the mean distance between each individual chemical bond present in the TNT molecule. This suggests that TNT behaves as an ideal diffusional species in RTIL solvents.

The results from the fitting also gave values for *nc*, the number of electrons multiplied by the concentration. The value of *n* = 1 was found for most RTILs, with the exception of [$P_{14,6,6,6}$][FAP], which gave closer to a 2-electron count. Unusual behaviour in RTILs with $[P_{14,6,6,6}]^+$ cations has been reported previously,[21,31] and is likely due to the extraction of H or H^+ from the cation.[32] We note that there may also be some errors in the concentration due to the very small volumes involved. The 1-electron reduction of TNT in most RTILs is in stark contrast to that observed in protic solvents, where a 6-electron (plus 6 proton) process is widely accepted (total 18 electrons and 18 protons over the three peaks).[1] In RTILs, the electron count has not been reported before, however, Xiao et al.[13] suggested that the same mechanism as in water occurs in RTILs, with the protons coming from either the solvent (e.g. acidic proton on the imidazolium ion) or from water molecules

in the RTIL. Since we have found the same electron count in most RTILs (even with imidazolium cations, where mildly acidic protons are available in the C(2) position),[33] we believe that the 1-electron count applies for TNT reduction in RTILs. Additionally, our experimental set-up (with the RTIL under vacuum conditions) allows the removal of trace water, leaving only water that is structurally bound to the RTILs,[34] which is unlikely to participate in follow-up chemical reactions. The suggestion of a 1-electron reduction process for peak I in RTILs is further supported by digital simulation of experimental voltammograms, as described in section 3.5.

3.3. Cyclic voltammetry of TNT reduction in RTILs on a TFE.

In order to investigate the mechanism further, the electrochemical behaviour over a wide concentration range should be studied. However, the experimental set-up on the microdisk electrode requires at least 20 μL of RTIL solvent (to connect the electrodes) meaning that high concentration solutions would require a large amount of TNT for each experiment. Therefore, thin film electrodes (TFEs) were employed to minimise the volume required to only 1.5 μL per experiment. The advantages of these electrodes for miniaturising experimental set-ups to allow the use of only a few microlitres of RTIL solvents have been described by our group recently.[35]

Figure 2 shows CVs for the reduction of TNT in eight RTILs on a gold TFE (radius = 0.5 mm) at a scan rate of 100 mVs^{-1}. Three reduction peaks were observed in all RTILs, similar to the microdisk electrode, likely to be the reduction of each of the three nitro groups present on TNT. The relative ratios of the three peaks are generally quite similar to that on the microdisk electrode (Figure 1), but the differences are reflected by the diffusion regimes to the two electrodes (i.e. slightly more radial diffusion present on the microdisk electrode compared to the macrodisk electrode). However, the main difference in the CVs is the less obvious oxidation back-peaks on the TFE, particularly when the potential is scanned over all three reduction peaks. For example, in $[C_4mim][NTf_2]$ on a TFE (Figure 3b), the three reduction peaks are observed, but very indistinct

reverse peaks, whereas in the same RTIL on a microdisk electrode (Figure 1b), the three reverse peaks are clearly seen. When the potential is reversed after each peak, the reverse peaks are much more obvious (see thinner CVs in Figure 3).

The behaviour at different scan rates (0.01 - 4 Vs^{-1}) was also studied (Figure S4). As with the microdisk electrode, a highly linear relationship of peak current (peak I) against the square root of scan rate in (most) RTILs on TFEs suggests that the electrochemical reduction process is diffusion controlled. In the more viscous RTILs at the highest scan rates, the peaks became very broad and indistinct, probably due to increased Ohmic drop. Additionally, CVs in $[C_6mim][FAP]$ showed (reproducible) evidence of fouling/passivation on the surface. It is unknown why this occurs, but non-ideal behaviour in $[FAP]^-$ RTILs has also been reported previously.[36,37]

The potentials of peaks I, II and III were also calculated relative to the mid-point of the Fc/Fc^+ redox couple (CVs shown in Figure S5), and are reported in Table 1. Similar to that observed on the microdisk electrode, the potential of peak I is the lowest for RTILs with imidazolium cations (-0.99 to -1.04 V), compared to pyrrolidinium (-1.07 V) and tetraalkylphosphonium (-1.20 to -1.21 V). The larger difference for the phosphonium cations (compared to the difference on the microdisk electrode) is probably due to increased Ohmic drop contributions on the mm-sized TFE in the highly viscous (highly resistive) $[P_{14,6,6,6}]^+$ RTILs. Peak-to-peak separations (Table S1) for the three TNT reduction peaks generally indicated relatively fast kinetics of peak I, slower kinetics of peak II and even slower kinetics for peak III. It is noted that ΔE_p for Fc/Fc^+ is approximately 70-75 mV in six of the RTILs, but much larger (163 and 186 mV) in the two most viscous RTILs. Since this effect was not observed on the microdisk electrode, it is probably due to the increased Ohmic drop on the larger TFE as the result of higher currents produced during CV scans.

3.4 Study of the Reaction Mechanism and Products of TNT Reduction (peak I) in RTILs.

The voltammetry for TNT reduction (reversing after peak I) was studied at a range of concentrations. Only peak I was investigated due to the complicated follow-up chemistry likely at the more negative potentials of peaks II and III (discussed later). Figure 4 shows the reduction of TNT from 3-150 mM, with the reduction currents normalised to peak I. The peak potentials are also fixed at –1.02 V due to the unstable reference electrode, which enables us to easily compare the changing shape of the voltammograms. As the concentration is increased, the relative height of the reverse oxidation peak decreases, and the peak-to-peak separations increase. This suggests that something other than a simple 1-electron reduction mechanism is occurring. From the reduced peak height at higher concentrations, an EC_2 mechanism can be suggested.[38,39] Figure 5 shows one possible scheme for an EC_2 reduction mechanism of TNT in RTILs to form an azo product. It is also possible that other species (e.g. azoxy products) may be formed, or further reactions of these products (e.g. to form short chain polymers) could occur after the electrochemical reduction, due to the presence of reactive radical species. CVs scanned over all three peaks (normalised to peak I, see Figure S6) show smaller currents for peaks II and III at higher concentrations, consistent with the removal of the radical anion of TNT more quickly at higher concentrations.

At higher concentrations of TNT (75 mM and above), a red solid was observed to deposit on the working electrode when scanning (just one scan) over peak I - an optical image of this deposit is shown in Figure S7. "Red colored products" were also reported by Forzani et al.[10] for TNT reduction in $[C_4mim][PF_6]$ at the potential of the third reduction peak. Our attempts to fully characterise the red solid were unsuccessful, in line with that reported by other research groups.[10,11] Nuclear Magnetic Resonance (NMR) spectroscopy, Fourier Transform Infrared (FTIR) spectroscopy and UV-Visible spectroscopy were attempted on the solution of TNT in $[C_4mim][NTf_2]$ before and after bulk electrolysis (see experimental details in the supporting information). However, even when TNT was present at very high concentrations in the RTIL (0.5 M), the RTIL ions were at such a high concentration that resulted in swamping the peaks from TNT. Separation of $[C_4mim][NTf_2]$ and TNT could not be easily achieved due to the non-volatile nature of the RTIL. The only technique

that produced a result without the RTIL swamping the TNT was UV-Visible spectroscopy, where it was observed that the normalized spectra of TNT after bulk electrolysis shifted to a longer wavelength (Figure S8). This suggests electronic transitions of lower energy thus an increase in conjugation of the electrogenerated product, supporting the possibility of dimerization, where a higher degree of conjugation is expected compared to TNT itself.[8] However, there is a lack of peak(s) in the visible range (~400-700 nm) despite the red-colored solid observed. It is possible that aggregation occurs while in a solid form, and when added to acetonitrile it disaggregates; therefore does not appear as a peak in the UV-VIS spectra. It is noted that the electrogenerated red solid could be dissolved in the RTIL simply by mixing (e.g. via pipetting) or by leaving for a sufficient time (e.g. more than 1 hour) to dissipate naturally.

3.5 Modelling the reduction of TNT in [C_4mim][NTf_2] using DigiSim®

The one-dimensional simulation program DigiSim® 3.03 (BAS Technicol)[40] was used to model the cyclic voltammograms for TNT reduction (peak I) at different concentrations. A simplified reaction mechanism was input into the simulation program:

$$A + e^- = B \qquad \textbf{(I)}$$

$$B + B = D \qquad \textbf{(II)}$$

where A is TNT, B is the radical anion of TNT and D is the dimer (e.g. azo or azoxy compound). Concentrations ranging from 3 mM to 150 mM were simulated using the planar diffusion model (appropriate for mm-sized electrodes in RTILs). A second heterogeneous step (reduction of species B) was also added to the simulation in order to better fit the current in the diffusion-limited region of peak I (i.e. due to the onset of peak II). Fig. 6 shows the overlaid experimental and best-fit simulated voltammograms for 3, 20, 42 and 75 mM TNT. An overlay of the normalized simulated voltammetry at the four concentrations is given in Figure S9. It was not possible to fit the experimental data at 116 mM and above due to deviations in the shape of the reverse peak, probably

as a result of surface passivation at these high concentrations. For the remaining concentration range (3 to 75 mM), the final parameters used in the simulation are given in Table 3. There is also evidence of passivation for the 75 mM scan, as evidenced in the poorer fitting of the reverse peak in Figure 6, consistent with the observation of the red solid after one CV scan at this concentration. The limiting processes were found to be the equilibrium constant and the rate of reaction of the chemical step. The electrochemical rate constant that gave the best fit over the concentration range was 5.0×10^{-2} cm s^{-1}. The reasonable fitting (particularly for the reduction currents) over the wide concentration range supports the suggestion of a 1-electron reduction process, and the general trend in the CVs (decreased back-peak current and increased ΔE_p, see Figure S9) is consistent with a follow-up dimerization reaction (i.e. EC_2 mechanism). We note that is highly possible that there may be other chemical reactions due to the presence of highly reactive radical species (e.g. forming short-chain polymer products, with azo and/or azoxy groups), but the simulation is merely a guide to support the suggested simple EC_2 reaction mechanism. Attempts were also made to simulate over all three peaks for one concentration (3 mM) using three successive 1-electron reduction processes (see Figure S10a), each coupled with dimerization reactions, but the currents for peaks II and III were too small. Therefore, 2-electron processes were considered for peaks II and III, but it resulted in peak currents that were too large in the forward and reverse scans (Figure S10b). The most reasonable fit was obtained if an EC_2E reaction was considered for peak III (see Figure S10c). It is also possible that more complicated reaction mechanisms occur at these negative potentials, but there is clear evidence that the three 6 electron processes that occur in water do not take place in RTILs.

4. Conclusions

The reduction of TNT has been studied in eight RTILs on Au microdisk and thin-film electrodes. Three reduction peaks were observed on both surfaces, with relatively fast (electrochemical) kinetics suggested for peak I (similar to ferrocene), slightly slower kinetics for peak II and even slower kinetics for peak III. TNT was found to obey the Stokes-Einstein relationship in RTILs (diffusion coefficient inversely proportional to solvent viscosity), with the gradient consistent with the calculated hydrodynamic radius of the molecule. The electron count revealed that the reduction proceeds by a 1-electron reduction in most RTILs, in contrast to the 6-electron reduction in water. At higher concentrations, relative ratios of reductive and oxidative peaks for peak I suggested a possible EC_2 reaction mechanism, which was supported by the formation of a red solid on the electrode at high concentrations, and also by digital simulation of the voltammograms. Although the EC_2 mechanism is not likely to occur at low concentrations (e.g. trace TNT concentrations that are used for analytical applications), the knowledge of the reduction mechanism of TNT in RTILs is very important for applications where TNT is present in high concentrations in the RTIL.

Supporting Information

CVs for the reduction of TNT at a range of scan rates in eight RTILs on: (a) a gold TFE and (b) a gold microelectrode, and also in the presence of ferrocene. Experimental and fitted chronoamperometric transients for TNT reduction in eight RTILs on a gold microelectrode, and CVs for TNT reduction (all three peaks) at a range of concentrations, normalised to peak I. An optical image of the TFE showing the red electrogenerated product and a UV-Vis plot of TNT (in the RTIL) before and after bulk electrolysis are attached. This material is available free of charge via the Internet at http://pubs.acs.org.

Author Information

Corresponding Author - E-mail: d.silvester-dean@curtin.edu.au

Author Contributions

C.K. performed the electrochemical experiments and data analysis. J. L. performed the simulations (DFT and DigiSim®) and made the figures for publication. D.S.S. conceived the ideas and wrote the manuscript with contributions of the other authors. All authors have given approval to the final version of the manuscript.

Acknowledgements

The authors thank the group of Professor Christopher Hardacre for kind donation of some of the ionic liquids used in this work. D.S.S. thanks the Australian Research Council for funding via a Discovery Early Career Research Award (DE120101456).

Tables

Table 1. Voltammetric Data (at 100 mVs^{-1}) for TNT Reduction in Eight RTILs: Reduction Potentials for Peaks I, II and III (vs. the Midpoint of Fc/Fc^{+}).

RTIL	*E* (vs. Fc/Fc^{+}) / V					
	μ- disk electrode			TFE		
	Peak I	Peak II	Peak III	Peak I	Peak II	Peak III
$[C_2mim][NTf_2]$	-1.06	-1.29	-1.60	-1.04	-1.28	-1.53
$[C_4mim][NTf_2]$	-1.06	-1.33	-1.67	-1.04	-1.30	-1.54
$[C_6mim][FAP]$	-1.06	-1.37	-1.72	-0.99	-1.31	-1.61
$[C_4mpyrr][NTf_2]$	-1.09	-1.45	-1.72	-1.07	-1.44	-1.69
$[C_4mim][BF_4]$	-1.01	-1.28	-1.52	-1.00	-1.26	-1.49
$[C_4mim][PF_6]$	-1.01	-1.26	-1.48	-1.00	-1.25	-1.54
$[P_{14,6,6,6}][NTf_2]$	-1.13	-1.66	-1.99	-1.20	-1.66	-2.04
$[P_{14,6,6,6}][FAP]$	-1.14	-1.62	-2.01	-1.21	-1.87	-2.24

Table 2. Viscosity, η, of Eight RTILs[41] and Diffusion Coefficients of TNT, D_{TNT}, Calculated From Chronoamperometric Fittings to the Shoup and Szabo Equation.[19]

RTIL	η / cP at 293 K	D_{TNT} / x 10^{-11} m^2 s^{-1}
$[C_2mim][NTf_2]$	34	4.1
$[C_4mim][NTf_2]$	52	2.6
$[C_6mim][FAP]$	74	1.6
$[C_4mpyrr][NTf_2]$	89	1.7
$[C_4mim][BF_4]$	112	1.1
$[C_4mim][PF_6]$	371	0.75
$[P_{14,6,6,6}][NTf_2]$	450	0.86
$[P_{14,6,6,6}][FAP]$	464	0.71

Table 3. Parameters Used in the Simulation of TNT Reduction (Peak I) Using DigiSim®. A Second Heterogeneous Step was Added due to the Onset of Peak II (in the Diffusion Limited Region of Peak I).

Heterogeneous	E_0 / V	α / λ	k_0 / cm s^{-1}
(I) A + e = B	-1.00	0.5	0.05
(II) B + e = C	-1.25	0.5	0.005

Homogeneous	K_{eq}	k_f / M^{-1} s^{-1}
B + B = D	3200	5500

Diffusion Coefficients

Species	D / × 10^{-11} m^2 s^{-1}	Species	D / × 10^{-11} m^2 s^{-1}
A	3.3	C	1.0
B	2.5	D	0.3

[a] Scan Rate, υ = 100 mVs^{-1}, working electrode area, A = 7.85×10^{-5} m^2

[b] Ru = 1400 Ω, Cdl = 2×10^{-7}

[c] E_0 was varied to match the experimental data (due to the use of an unstable reference electrode).

Figures

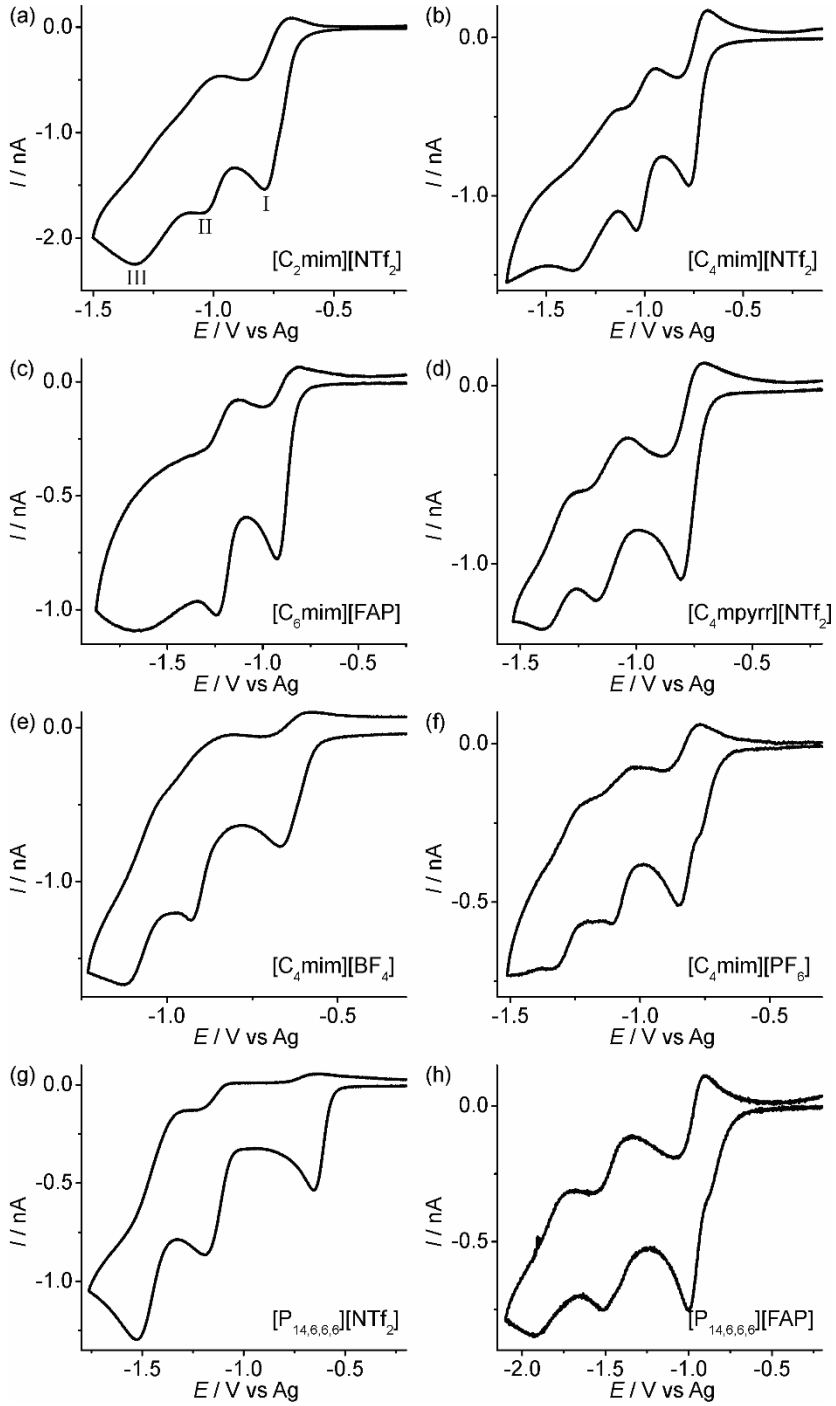

Figure 1. CV (100 mVs^{-1}) of the reduction of TNT (3 mM) on a gold microelectrode in a) $[C_2mim][NTf_2]$, b) $[C_4mim][NTf_2]$, c) $[C_6mim][FAP]$, d) $[C_4mpyrr][NTf_2]$, e) $[C_4mim][BF_4]$, f) $[C_4mim][PF_6]$, g) $[P_{14,6,6,6}][NTf_2]$, and h) $[P_{14,6,6,6}][FAP]$.

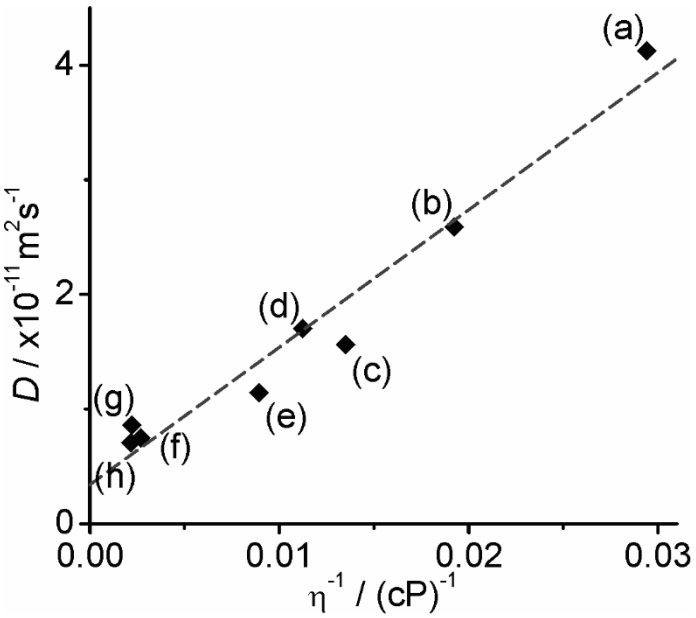

Figure 2. Diffusion coefficient (D) of TNT against the inverse of viscosity (η^{-1}) for eight RTILs: a) $[C_2mim][NTf_2]$, b) $[C_4mim][NTf_2]$, c) $[C_6mim][FAP]$, d) $[C_4mpyrr][NTf_2]$, e) $[C_4mim][BF_4]$, f) $[C_4mim][PF_6]$, g) $[P_{14,6,6,6}][NTf_2]$, and h) $[P_{14,6,6,6}][FAP]$. Dashed line indicates line of best fit.

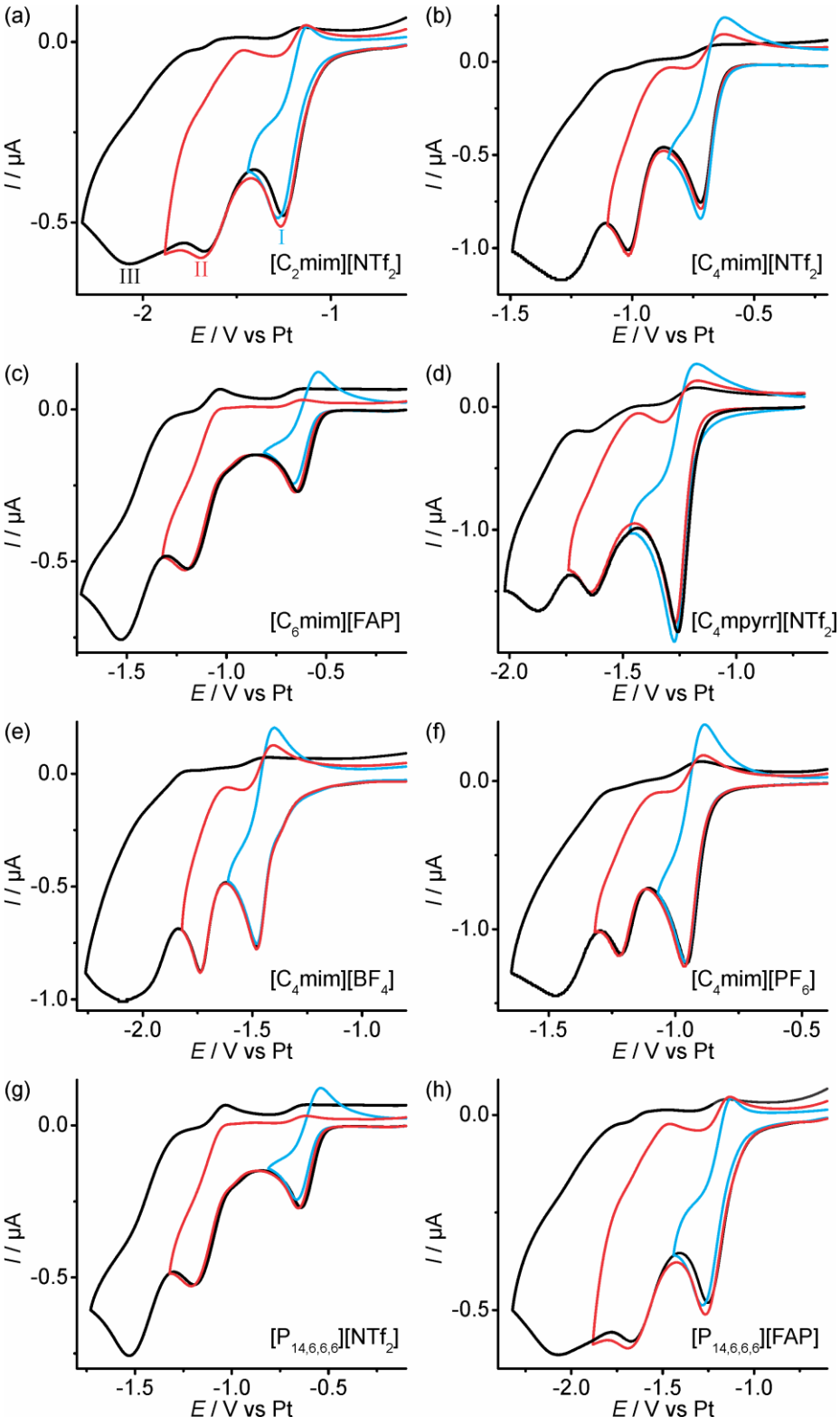

Figure 3. CV (100 mVs^{-1}) of the reduction of TNT (3 mM) with the scan reversed after peaks I, II, and III on a gold TFE in a) $[C_2mim][NTf_2]$, b) $[C_4mim][NTf_2]$, c) $[C_6mim][FAP]$, d) $[C_4mpyrr][NTf_2]$, e) $[C_4mim][BF_4]$, f) $[C_4mim][PF_6]$, g) $[P_{14,6,6,6}][NTf_2]$, and h) $[P_{14,6,6,6}][FAP]$.

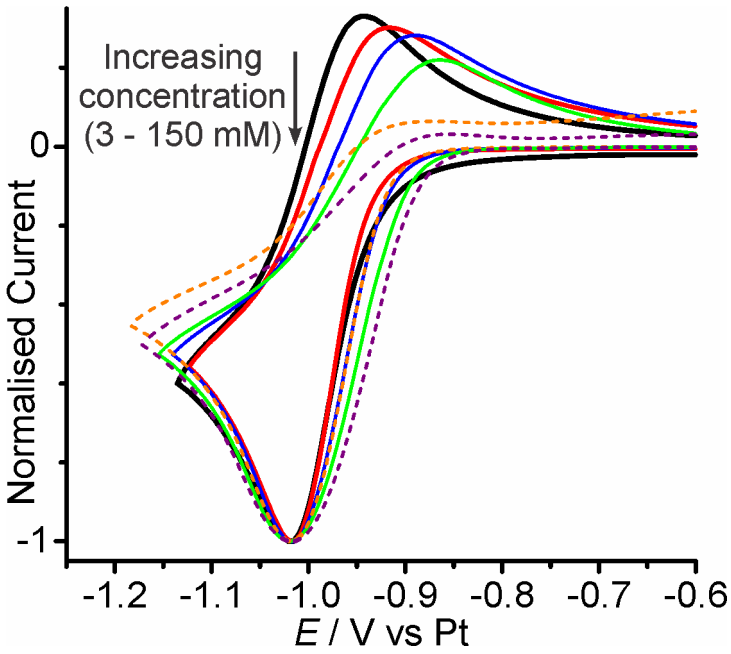

Figure 4. CV (100 mVs^{-1}) of TNT reduction at various concentrations (3 mM, 20 mM, 42 mM, 75 mM, 116 mM and 150 mM) reversed after peak I in $[C_4mim][NTf_2]$ on a gold TFE. The currents have been normalised to Peak I, and the reduction peak potentials shifted to -1.02 V due to the unstable reference electrode.

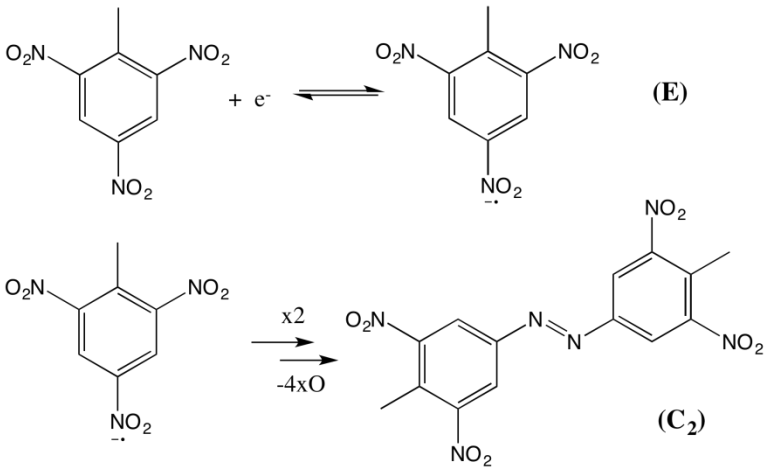

Figure 5. Simplified scheme of an EC_2 mechanism for TNT reduction, possibly forming an electrogenerated azo product.

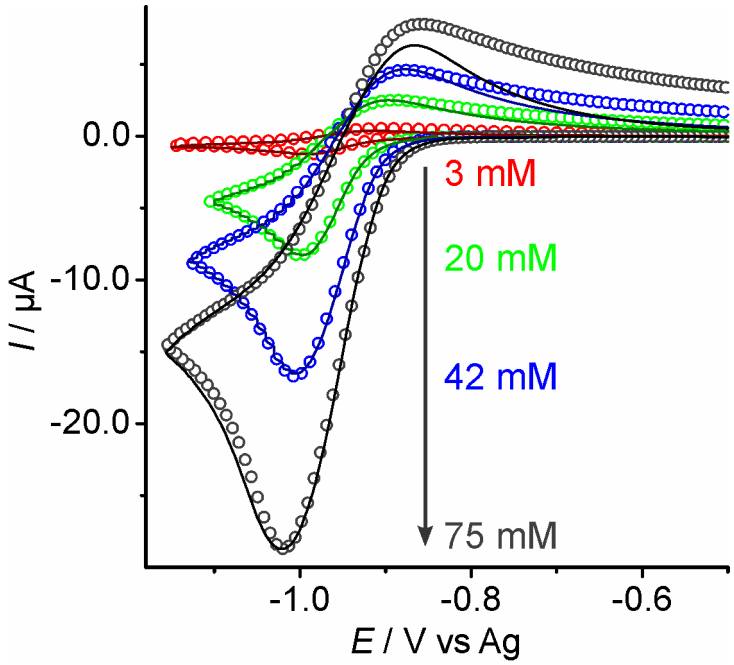

Figure 6. A comparison of experimental (–) and simulated (○) voltammograms for the reduction of 3, 20, 42, 75 mM TNT in $[C_4mim][NTf_2]$ at scan rates of 0.1 Vs^{-1}.

TOC Figure

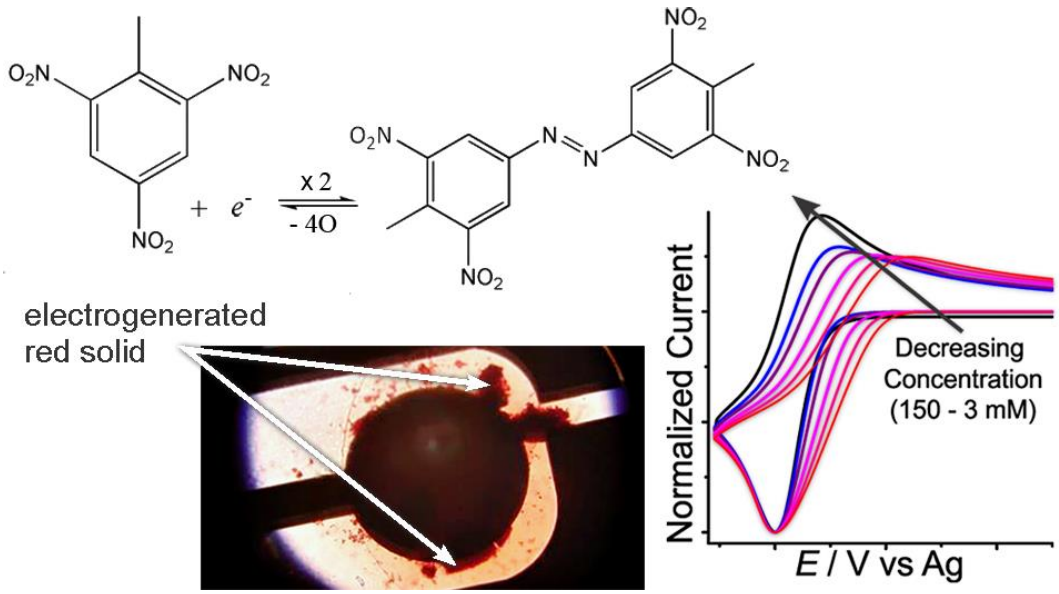
O_2N
NO_2
NO_2
+ e^-
x 2
- 4O
O_2N
N
N
NO_2
NO_2
NO_2
electrogenerated
red solid
Normalized Current
Decreasing
Concentration
(150 - 3 mM)
E / V vs Ag

References

(1) Chua, C. K.; Pumera, M.; Rulíšek, L. Reduction Pathways of 2,4,6-Trinitrotoluene: An Electrochemical and Theoretical Study *J. Phys Chem. C* **2012**, *116*, 4243-4251.

(2) Rabenecker, P.; Pinkwart, K. A Look Behind Electrochemical Detection of Explosives *Propellants Explos. Pyrotech.* **2009**, *34*, 274-279.

(3) Wang, J. Electrochemical Sensing of Explosives *Electroanalysis* **2007**, *19*, 415-423.

(4) Bratin, K.; Kissinger, P. T.; Briner, R. C.; Bruntlett, C. S. Determination of Nitro Aromatic, Nitramine, and Nitrate Ester Explosive Compounds in Explosive Mixtures and Gunshot Residue by Liquid Chromatography and Reductive Electrochemical Detection *Anal. Chim. Acta* **1981**, *130*, 295-311.

(5) de Sanoit, J.; Vanhove, E.; Mailley, P.; Bergonzo, P. Electrochemical Diamond Sensors for TNT Detection in Water *Electrochim. Acta* **2009**, *54*, 5688-5693.

(6) Fu, X.; Benson, R. F.; Wang, J.; Fries, D. Remote Underwater Electrochemical Sensing System for Detecting Explosive Residues in the Field *Sens. Act. B* **2005**, *106*, 296-301.

(7) Galik, M.; O'Mahony, A. M.; Wang, J. Cyclic and Square-Wave Voltammetric Signatures of Nitro-Containing Explosives *Electroanalysis* **2011**, *23*, 1193-1204.

(8) Chua, C. K.; Pumera, M. Influence of Methyl Substituent Position on Redox Properties of Nitroaromatics Related to 2,4,6-Trinitrotoluene *Electroanalysis* **2011**, *23*, 2350 – 2356.

(9) Prabu, H. G.; Talawar, M. B.; Mukundan, T.; Asthana, S. N. Studies on the Utilization of Stripping Voltammetry Technique in the Detection of High-Energy Materials *Combust. Explos. Shock Waves* **2011**, *47*, 87-95.

(10) Forzani, E. S.; Lu, D. L.; Leright, M. J.; Aguilar, A. D.; Tsow, F.; Iglesias, R. A.; Zhang, Q.; Lu, J.; Li, J. H.; Tao, N. J. A Hybrid Electrochemical-Colorimetric Sensing Platform for Detection of Explosives *J. Am. Chem. Soc.* **2009**, *131*, 1390-1391.

(11) Aguilar, A. D.; Forzani, E. S.; Leright, M.; Tsow, F.; Cagan, A.; Iglesias, R. A.; Nagahara, L. A.; Amlani, I.; Tsui, R.; Tao, N. J. A Hybrid Nanosensor for TNT Vapor Detection *Nano Lett.* **2010**, *10*, 380-384.

(12) Fernández, E.; Vidal, L.; Iniesta, J.; Metters, J. P.; Banks, C. E.; Canals, A. Screen-Printed Electrode-Based Electrochemical Detector Coupled with In-Situ Ionic-Liquid-Assisted Dispersive Liquid–Liquid Microextraction for Determination of 2,4,6-Trinitrotoluene *Anal. Bioanal. Chem.* **2014**, *406*, 2197-2204.

(13) Xiao, C.; Rehman, A.; Zeng, X. Dynamics of Redox Processes in Ionic Liquids and Their Interplay for Discriminative Electrochemical Sensing *Anal. Chem.* **2012**, *84*, 1416-1424.

(14) Bonhôte, P. A. D.; Papageorgiou, N.; Kalyanasundaram, K.; Grätzel, M. Hydrophobic, Highly Conductive Ambient-Temperature Molten Salts *Inorg. Chem.* **1996**, *35*, 1168-1178.

(15) MacFarlane, D. R.; Meakin, P.; Sun, J.; Amini, N. Pyrrolidinium Imides: A New Family of Molten Salts and Conductive Plastic Crystal Phases *J. Phys. Chem. B* **1999**, *103*, 4164-4170.

(16) Sharp, M. Determination of the Charge-Transfer Kinetics of Ferrocene at Platinum and Vitreous Carbon Electrodes by Potential Step Chronocoulometry *Electrochim. Acta* **1983**, *28*, 301-308.

(17) Silvester, D. S.; Wain, A. J.; Aldous, L.; Hardacre, C.; Compton, R. G. Electrochemical Reduction of Nitrobenzene and 4-Nitrophenol in the Room Temperature Ionic Liquid $[C_4dmim][N(Tf)_2]$. *J. Electroanal. Chem.* **2006**, *596*, 131-140.

(18) Lee, J.; Murugappan, K.; Arrigan, D. W. M.; Silvester, D. S. Oxygen Reduction Voltammetry on Platinum Macrodisk and Screen-Printed Electrodes in Ionic Liquids: Reaction of the Electrogenerated Superoxide Species with Compounds used in the Paste of Pt Screen-Printed Electrodes? *Electrochim. Acta* **2013**, *101*, 158-168.

(19) Shoup, D.; Szabo, A. Chronoamperometric Current at Finite Disk Electrodes *J. Electroanal. Chem.* **1982**, *140*, 237-245.

(20) Hilmi, A.; Luong, J. H. T.; Nguyen, A.-L. Development of Electrokinetic Capillary Electrophoresis Equipped with Amperometric Detection for Analysis of Explosive Compounds *Anal. Chem.* **1999**, *71*, 873-878.

(21) Rogers, E. I.; Silvester, D. S.; Poole, D. L.; Aldous, L.; Hardacre, C.; Compton, R. G. Voltammetric Characterization of the Ferrocene|Ferrocenium and Cobaltocenium|Cobaltocene Redox Couples in RTILs. *J. Phys. Chem. C* **2008**, *112*, 2729-2735.

(22) Barnes, A. S.; Rogers, E. I.; Streeter, I.; Aldous, L.; Hardacre, C.; Compton, R. G. Extraction of Electrode Kinetic Parameters from Microdisc Voltammetric Data Measured under Transport Conditions Intermediate between Steady-State Convergent and Transient Linear Diffusion As Typically Applies to Room Temperature Ionic Liquids *J. Phys. Chem. B* **2008**, *112*, 7560-7565.
(23) Compton, R. G.; Banks, C. E.: *Understanding Voltammetry*; 1st. Ed., World Scientific: Singapore, 2007.
(24) Lovelock, K. R. J.; Ejigu, A.; Loh, S. F.; Men, S.; Licence, P.; Walsh, D. A. On the Diffusion of Ferrocenemethanol in Room-Temperature Ionic Liquids: An Electrochemical Study *Phys. Chem. Chem. Phys.* **2011**, *13*, 10155-10164.
(25) Taylor, A. W.; Licence, P.; Abbott, A. P. Non-Classical Diffusion in Ionic Liquids *Phys. Chem. Chem. Phys.* **2011**, *13*, 10147-10154.
(26) Vorotyntsev, M. A.; Zinovyeva, V. A.; Picquet, M. Diffusional Transport in Ionic Liquids: Stokes–Einstein Relation or "Sliding Sphere" Model? Ferrocene (Fc) in Imidazolium Liquids *Electrochim. Acta* **2010**, *55*, 5063-5070.
(27) Barrosse-Antle, L. E.; Silvester, D. S.; Aldous, L.; Hardacre, C.; Compton, R. G. Electroreduction of Sulfur Dioxide in Some Room-Temperature Ionic Liquids. *J. Phys. Chem. C* **2008**, *112*, 3398-3404.
(28) Buzzeo, M. C.; Hardacre, C.; Compton, R. G. Use of Room Temperature Ionic Liquids in Gas Sensor Design *Anal. Chem.* **2004**, *76*, 4583-4588.
(29) Silvester, D. S.; Ward, K. L.; Aldous, L.; Hardacre, C.; Compton, R. G. The Electrochemical Oxidation of Hydrogen at Activated Platinum Electrodes in Room Temperature Ionic Liquids as Solvents *J. Electroanal. Chem.* **2008**, *618*, 53-60.
(30) Silvester, D. S.; Uprety, S.; Wright, P. J.; Massi, M.; Stagni, S.; Muzzioli, S. Redox Properties of a Rhenium Tetrazolato Complex in Room Temperature Ionic Liquids: Assessing the Applicability of the Stokes−Einstein Equation for a Metal Complex in Ionic Liquids *J. Phys. Chem. C* **2012**, *116*, 7327-7333.
(31) Evans, R. G.; Klymenko, O. V.; Saddoughi, S. A.; Hardacre, C.; Compton, R. G. Electroreduction of Oxygen in a Series of Room Temperature Ionic Liquids Composed of Group 15-Centered Cations and Anions *J. Phys. Chem. B* **2004**, *108*, 7878-7886.
(32) Li, P.; Barnes, E. O.; Hardacre, C.; Compton, R. G. Microelectrode Voltammetry of Dioxygen Reduction in a Phosphonium Cation-Based Room-Temperature Ionic Liquid: Quantitative Studies *J. Phys. Chem. C* **2015**, *119*, 2716-2726.
(33) De Vos, N.; Maton, C.; Stevens, C. V. Electrochemical Stability of Ionic Liquids: General Influences and Degradation Mechanisms *ChemElectroChem* **2014**, *1*, 1258-1270.
(34) Reid, J. E. S. J.; Walker, A. J.; Shimizu, S. Residual Water in Ionic Liquids: Clustered or Dissociated? *Phys. Chem. Chem. Phys.* **2015**, *17*, 14710-14718.
(35) Lee, J.; Du Plessis, G.; Arrigan, D. W. M.; Silvester, D. S. Towards Improving the Robustness of Electrochemical Gas Sensors: impact of PMMA Addition on the Sensing of Oxygen in an Ionic Liquid *Anal. Methods* **2015**, *7*, 7327-7335.
(36) Kuberský, P.; Altšmíd, J.; Hamáček, A.; Nešpůrek, S.; Zmeškal, O. An Electrochemical NO2 Sensor Based on Ionic Liquid: Influence of the Morphology of the Polymer Electrolyte on Sensor Sensitivity *Sensors* **2015**, *15*, 28421-28434.
(37) Murugappan, K.; Silvester, D. S. Electrochemical Studies of Hydrogen Chloride Gas in Several Room Temperature Ionic Liquids: Mechanism and Sensing *Phys. Chem. Chem. Phys.* **2016**, *18*, 2488-2494.
(38) Compton, R. G.; Mason, D.; Unwin, P. R. Rotating-Disc Electrode Voltammetry: Waveshape Analysis for DISP2 and EC2 Processes *J. Chem. Soc., Faraday Trans.* **1988**, *84*, 473-482.
(39) Eswari, A.; Rajendran, L. Mathematical Modeling of Cyclic Voltammetry for EC2 Reaction *Russian J. Electrochem.* **2011**, *47*, 191-199.
(40) Rudolph, M.; Reddy, D. P.; Feldberg, S. W. A Simulator for Cyclic Voltammetric Responses *Anal. Chem.* **1994**, *66*, 589-600.
(41) Barrosse-Antle, L. E.; Bond, A. M.; Compton, R. G.; O 'Mahony, A. M.; Rogers, E. I.; Silvester, D. S. Voltammetry in Room Temperature Ionic Liquids: Comparisons and Contrasts with Conventional Electrochemical Solvents *Chem. Asian J.* **2010**, *5*, 202-230.